NEOCLASSICAL TRANSPORT IN STELLARATORS – FURTHER RESULTS FROM AN INTERNATIONAL COLLABORATION

C.D. Beidler[1], S.V. Kasilov[2], W. Kernbichler[3], H. Maaßberg[1], D.R. Mikkelsen[4], S. Murakami[5], V.V. Nemov[2], M. Schmidt[1], D.A. Spong[6], V. Tribaldos[7], A. Wakasa[8], R.B. White[4]

[1]*Max-Planck-Institut für Plasmaphysik, IPP–EURATOM Association, Greifswald, GERMANY*
[2]*Institute of Plasma Physics, NSC 'Kharkov Institute of Physics and Technology', Kharkov, UKRAINE*
[3]*Technische Universität Graz, ÖAW–EURATOM Association, Graz, AUSTRIA*
[4]*Princeton Plasma Physics Laboratory, Princeton NJ, USA*
[5]*Department of Nuclear Engineering, Kyoto University, Kyoto, JAPAN*
[6]*Oak Ridge National Laboratory, Oak Ridge TN, USA*
[7]*Laboratorio Nacional de Fusión, Asociación EURATOM–CIEMAT para Fusión, Madrid, SPAIN*
[8]*Graduate School of Engineering, Hokkaido University, Sapporo, JAPAN*

A broad-based effort is currently underway to provide a comprehensive description of the neoclassical transport processes relevant to plasma performance in stellarator experiments. Briefly summarized, the principal goals of this effort are: (1) A thorough benchmarking of the various methods used to calculate neoclassical transport coefficients. These include (where appropriate): analytic theory, field-line integration techniques, Monte Carlo simulations, and numerical solutions of the ripple-averaged and drift kinetic equations. (2) The description of the benchmarking results by means of an efficient "neoclassical data base" to facilitate the analysis of experimental results and to provide an interface for predictive transport codes.

The devices under investigation are representative of the extensive configuration space available to stellarators: the classical heliotron/torsatron Large Helical Device (LHD), in operation at Toki, Japan; the heliac TJ-II, in operation at Madrid, Spain; the quasi-axisymmetric National Compact Stellarator Experiment (NCSX), in the engineering design phase at Princeton, USA; the Quasi-Poloidally Symmetric device (QPS), in the planning stage at Oak Ridge, USA, and two advanced stellarators of the Wendelstein line, W7-AS which recently ended operation at Garching, Germany, and the helias W7-X which is under construction at Greifswald, Germany.

Initial results from the international collaboration were reported during the previous Stellarator Workshop in Canberra, Australia; the present paper gives a summary of more recent progress.

Basics — The *local* ansatz which underlies neoclassical transport theory allows an ordering of the drift kinetic equation in which the minor-radius and energy coordinates appear only as parameters, reducing a nominally 5D problem to a more manageable 3D. Additionally, it becomes possible to characterize all neoclassical effects in terms of three *mono-energetic* coefficients describing the radial transport, the bootstrap current and the parallel conductivity; the full neoclassical transport matrix is subsequently obtained through the appropriate convolutions of the mono-energetic coefficients with a local Maxwellian. For benchmarking, it is thus sufficient to determine and compare the mono-energetic quantities of interest.

Benchmarking — The most general methods for determining neoclassical transport coefficients are numerical algorithms which solve the full drift kinetic equation and include a number of schemes based on the Monte Carlo approach [1-3] as well as the DKES (Drift Kinetic Equation Solver) code which employs a variational principle where the solution is expressed using a series of Fourier-Legendre test functions [4]. These algorithms demand a considerable price in computational resources, however, prompting the development of efficient methods for solving "simplified" kinetic equations. As examples, the field-line-integration technique embodied in the NEO code [5] is valid for arbitrarily complex magnetic fields in the asymptotic $1/\nu$ regime (radial transport inversely proportional to the collision frequency), whereas the General Solution of the Ripple Averaged Kinetic Equation (GSRAKE) [6] may be employed throughout the entire long-mean-free-path *(lmfp)* regime but only for magnetic fields which are accurately described within the so-called "multiple-helicity" model for B [7].

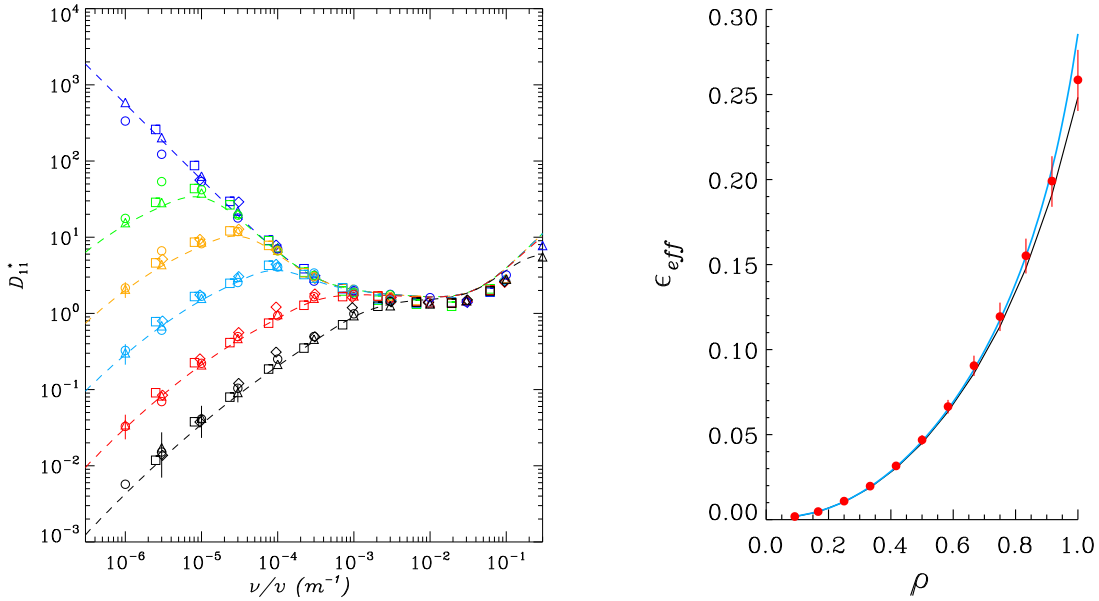

Figure 1. Benchmarking results for the standard configuration of LHD. On the left, the normalized radial transport coefficient is plotted versus the inverse mean free path ν/v (m^{-1}) assuming normalized values of the radial electric field to be $|E|/vB_0 = 3 \times 10^{-3}$, 1×10^{-3}, 3×10^{-4}, 1×10^{-4}, 3×10^{-5} and zero. Numerical results for the $\rho = 0.5$ flux surface are depicted by: triangles for DKES, circles [1], squares [2] and diamonds [3] for the Monte Carlo simulations, and by the dashed curves for GSRAKE. On the right, the effective helical ripple for $1/\nu$ transport is shown as a function of the normalized minor radius. Analytical results are shown by the black curve, those from NEO in light blue and the DKES calculations are given by red data points with upper and lower bounds indicated by the 'error bars'.

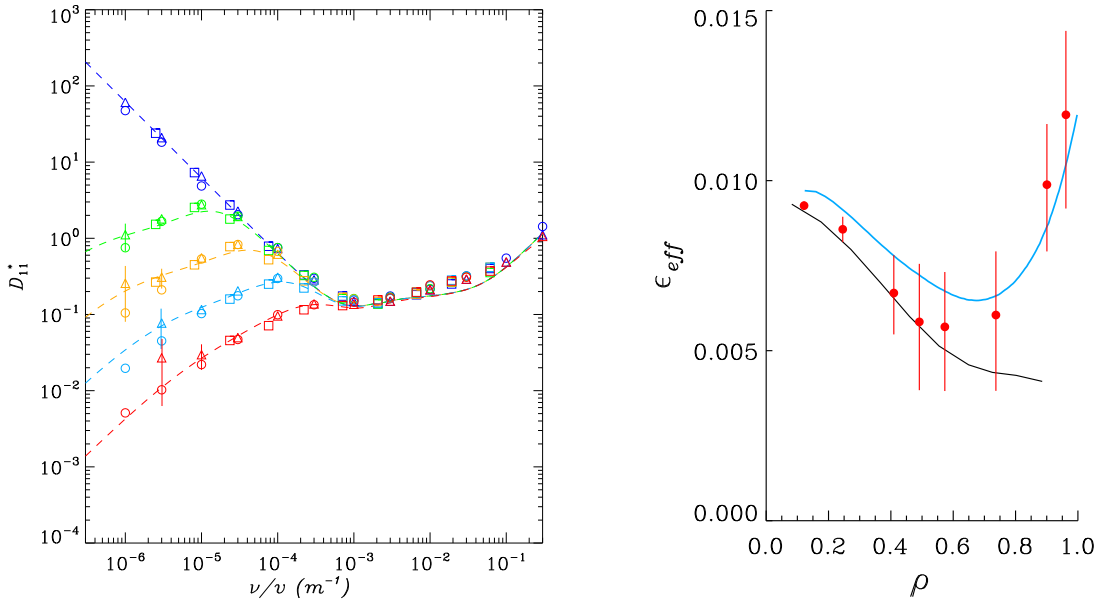

Figure 2. Benchmarking results for the standard configuration of W7-X. On the left, the normalized radial transport coefficient is plotted versus the inverse mean free path for the $\rho = 0.25$ flux surface. On the right, the effective helical ripple for $1/\nu$ transport is shown as a function of the normalized minor radius. In both plots, the symbols and color coding are the same as used in figure 1.

An example of benchmarking results is given in figure 1 for the standard configuration of the LHD, a device for which all the methods described above are applicable. On the left, the mono-energetic radial transport coefficient, normalized to the plateau value of the equivalent axisymmetric tokamak (with circular flux surfaces), D_{11}^*, is plotted as a function of inverse mean free path, ν/v, where v is the velocity of the mono-energetic test particles considered; the flux surface at half the plasma radius has been chosen. Six different values of the radial electric field have been considered, illustrating the strong dependence of D_{11}^* on this quantity in the *lmfp* regime. Results from DKES, three Monte Carlo codes and GSRAKE are compared; excellent agreement is obtained in all cases considered. On the right, the radial dependence of the *effective* helical ripple for $1/\nu$ transport determined using DKES, NEO and an analytic expression [8] is plotted; again the agreement is excellent.

A further sample of the benchmarking results is shown in figure 2 for the standard configuration of W7-X. In this device, the principal magnetic field harmonics have been chosen to provide a very-low level of radial transport. This optimization is verified for the inner flux surfaces but suffers a modest degradation further out due to the presence of small additional terms in the magnetic field spectrum; accurate estimates of the transport at these radii require numerical methods which account for the full complexity of B (observe the predicted radial profiles of ϵ_{eff}).

DKES is currently the only numerical tool available for determining the bootstrap current coefficient in stellarators at arbitrary values of collision frequency and radial electric field. Its results may, however, be compared with the analytic formula of Shaing and Callen [9] valid in the collisionless limit. A sample of the results is provided in figure 3, in which the mono-energetic bootstrap current coefficient, normalized to the limiting value of the equivalent axisymmetric tokamak (with circular flux surfaces), D_{31}^*, is plotted as a function of inverse mean free path; results for the flux surface at half the plasma radius are depicted for the standard configurations of LHD, W7-X, NCSX and W7-AS. The theoretical prediction for $\nu \to 0$ is indicated by the dashed line. These results show a rather complicated dependence of D_{31}^* on the value of the radial electric field for experimentally relevant values of ν/v; a theoretical explanation of this behavior is currently lacking. The analytic predictions for the value of D_{31}^* in the collisionless limit are supported reasonably well by the numerical results, although one notes that this collisionless limit is approached rather slowly.

Semi-Analytic Description of the Radial Transport — Benchmarking of the radial transport coefficient has been successfully completed for all configurations listed in the introduction of this paper. The results exhibit common qualitative features and may be accurately described by employing least-squares fits to quantities which appear in a physics-based, semi-analytic model for D_{11}^* originally developed for classical stellarators. The model characterizes the transport as a sum of three terms, $D_{11} = D_{axi} + D_{lmfp} + D_{add}$, where D_{axi} contains the usual Pfirsch-Schlüter, plateau and banana regimes expected for the axisymmetric field $B/B_0 = 1 + b_T \cos\theta$ (for a stellarator, these losses are only relevant when the mean free path is short), D_{lmfp} describes the stellarator-specific long-mean-free-path regime and D_{add} is an "additional" contribution relevant only when $D_{axi} \approx D_{lmfp}$. The fitting is done in two steps, beginning with the results obtained for zero electric field. Here, D_{lmfp} is given by the asymptotic $1/\nu$ result (with ϵ_{eff} determined by NEO) and least-squares fitting is used to determine "best" values of b_T and the two free coefficients (magnitude and saturation) in D_{add}. With this step completed, D_{lmfp} is then found for arbitrary values of the electric field by means of an extremely efficient solution of the bounce-averaged kinetic equation assuming $B/B_0 = 1 + b_T \cos\theta - \epsilon_h(1 - \sigma\cos\theta)\cos\eta$, which is the simplest model field capable of describing strong drift optimization [10]. Least-squares fitting is now carried out to determine values of ϵ_h, σ and a third quantity appearing in the boundary conditions (physically, this quantity controls the importance of collisionless trapping and detrapping in the local ripples of B).

Benchmarking results and their semi-analytic fits are presented in figure 4 for each of the configurations considered here. These illustrate a number of points which are worth mentioning. The inward-shifted LHD has a very high degree of drift optimization leading to an extended region in the *lmfp* regime where (for moderate values of the radial electric field) the radial transport is only a weak function of collision frequency. The departures from "true" symmetry which are inherent in the realization of a quasi-symmetric device such as

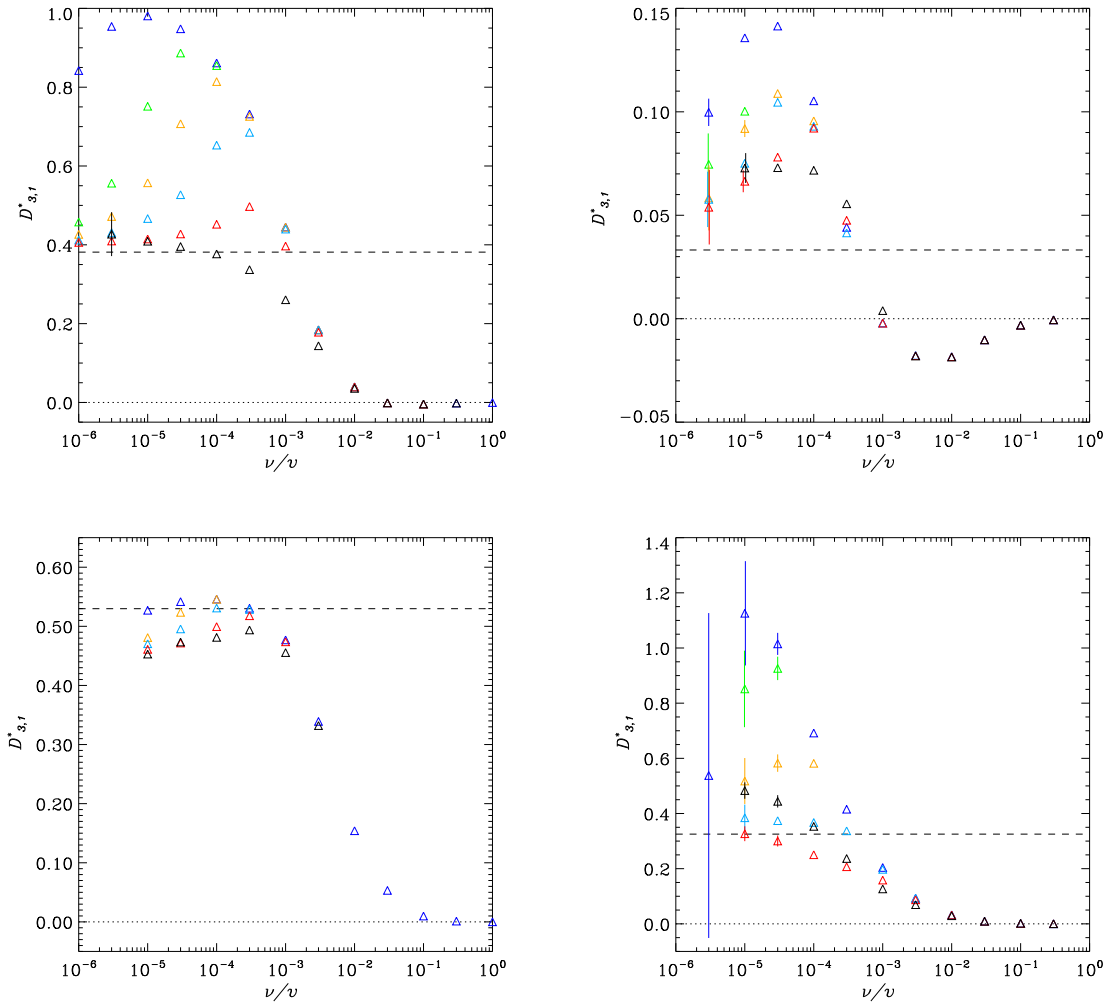

Figure 3. The normalized bootstrap current coefficient is shown as a function of inverse mean free path for the standard configurations of LHD (upper left), W7-X (upper right), NCSX (lower left) and W7-AS (lower right). DKES results for the $\rho = 0.5$ flux surface are depicted by triangles; color coding for the value of the radial electric field is the same as used in figure 1. The predicted value of $D^*_{3,1}$ in the collisionless limit [9] is shown by the dashed curve.

NCSX, lead to a qualitative behavior of the radial transport coefficient similar to that found in other stellarators. W7-AS and TJ-II both have rather complicated magnetic field spectra yet, nevertheless, their radial transport properties are accurately described using the comparatively simple model field and semi-analytic approach described above.

Acknowledgment

This work was (partly) supported by the Associations IPP-EURATOM, ÖAW-EURATOM and EURATOM-CIEMAT. The content of the publication is the sole responsibility of its publishers and it does not necessarily represent the views of the Commission or its services.

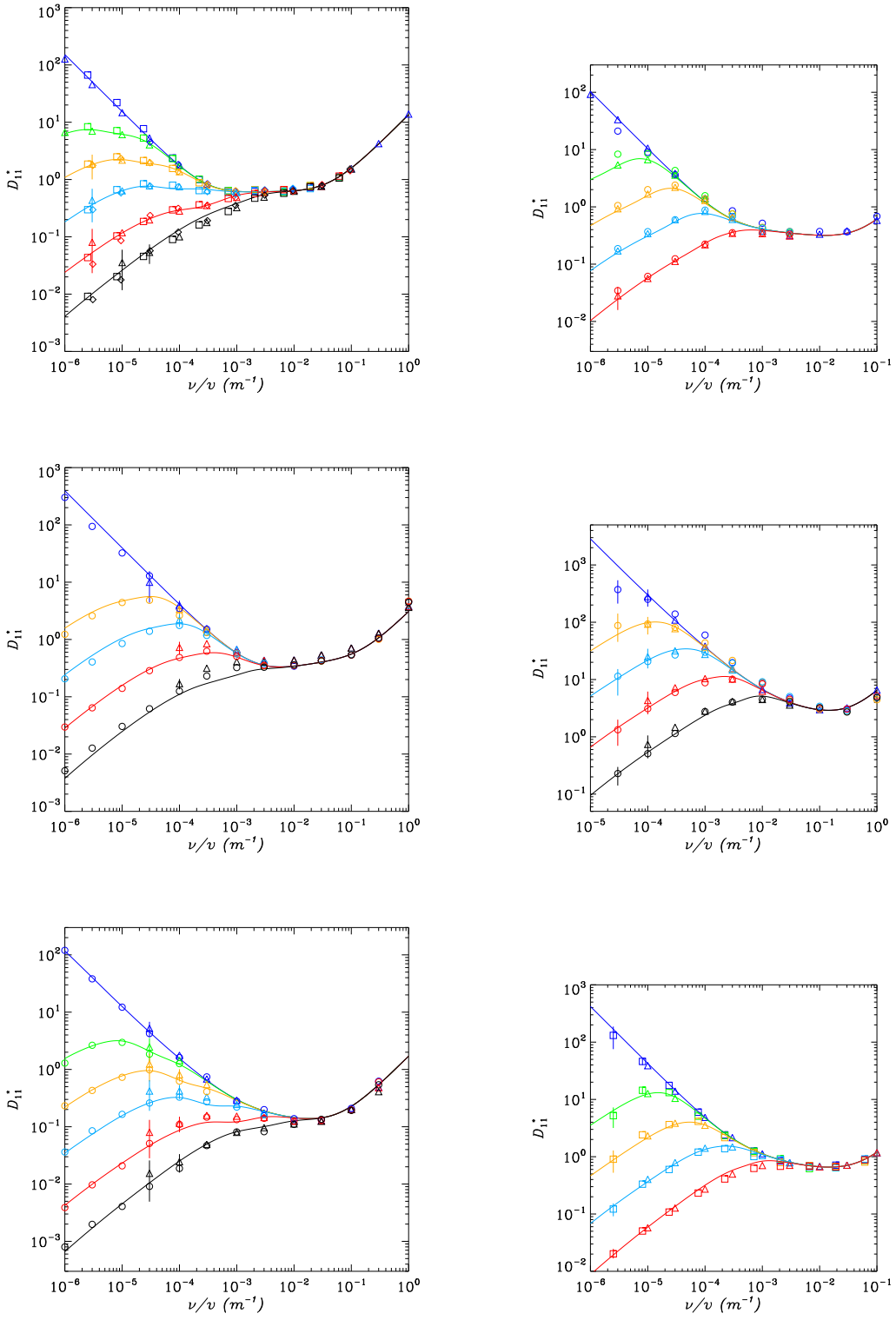

Figure 4. "Best fits" to the numerical results obtained from the semi-analytic description of radial transport are shown as continuous curves for the inward-shifted LHD (upper left), the low-mirror W7-X (upper right), and the standard configurations of NCSX (middle left), TJ-II (middle right), QPS (lower left) and W7-AS (lower right). The symbols and color coding are the same as used in figure 1.

References

[1] Tribaldos V 2001 *Phys. Plasmas* **8** 1229
[2] Beidler C D, Hitchon W N G and Shohet J L 1987 *J. Comput. Phys.* **72** 220
[3] Wakasa A *et al* 2001 *J. Plasma Fusion Res. SERIES* **4** 408
[4] van Rij W I and Hirshman S P 1989 *Phys. Fluids* B **1** 563
[5] Nemov V V, Kasilov S V, Kernbichler W and Heyn M F 1999 *Phys. Plasmas* **6** 4622
[6] Beidler C D and D'haeseleer W D 1995 *Plasma Phys. Control. Fusion* **37** 463
[7] Shaing K C and Hokin S A 1983 *Phys. Fluids* **26** 2136
[8] Beidler C D and Maaßberg H 2001 *Plasma Phys. Control. Fusion* **43** 1131
[9] Shaing K C and Callen J D 1983 *Phys. Fluids* **26** 3315
[10] Mynick H E, Chu T K and Boozer A H 1982 *Phys. Rev. Lett.* **48** 322